Controlling mesoscopic phase separation near electronic topological transitions via quenched disorder in ternary diborides

2008 J. Phys.: Condens. Matter 20 434222

(http://iopscience.iop.org/0953-8984/20/43/434222)

J. Phys.: Condens. Matter **20** (2008) 434222 (11pp) doi:10.1088/0953-8984/20/43/434222

Controlling mesoscopic phase separation near electronic topological transitions via quenched disorder in ternary diborides

Valerio Palmisano[1], Laura Simonelli[1], Alessandro Puri[1], Michela Fratini[1], Yan Busby[1], P Parisiades[2], Efthimios Liarokapis[2], Michela Brunelli[3], A N Fitch[3] and Antonio Bianconi[1]

[1] Department of Physics, La Sapienza University of Rome, Piazzale Aldo Moro 2, 00185 Roma, Italy
[2] Department of Applied Mathematics and Physics, National Technical University of Athens, GR-157 80 Athens, Greece
[3] European Synchrotron Radiation Facility, BP 220, F-38043, Grenoble Cedex, France

Received 7 July 2008
Published 9 October 2008
Online at stacks.iop.org/JPhysCM/20/434222

Abstract

A phase separation driven by the negative compressibility of the electron gas, near electronic topological transitions (ETT), could drive the system at the verge of a catastrophe. We show here that the metastable phases very close to the ETT transition are observed in a mesoscopic phase separation (MePhS) driven by the quenched lattice disorder. By using high resolution synchrotron radiation x-ray powder diffraction we have identified the MePhS for the intermetallic ternary $Mg_{1-x}Al_xB_2$ in the proximity of two ETTs: the first at $x_1 = 0.1$ and the second at $x_2 = 0.3$. We have identified the competition between a first 'relaxed' (R) hole poor and a second 'tense' (T) hole rich phase, and by micro-Raman we observe the splitting of the in-plane phonon E_{2g} mode in the proximity of the first ETT at $x = 0.1$. The anisotropic quenched disorder due to a random distribution of Al^{3+} and Mg^{2+} ions both in the axial (c axis) direction and planar (ab plane) direction, probed by x-ray diffraction and Raman data, is proposed to be the physical variable that allows the formation of metastable phases near the critical points of electronic topological transitions, where Feshbach shape resonances in interband pairing amplifies the superconducting critical temperature.

(Some figures in this article are in colour only in the electronic version)

1. Introduction

There are growing efforts to control mesoscopic phase separation (MePhS) for the development of novel functional complex materials with unique properties. Experimental evidence is accumulating that the emergence of unique highly correlated electronic phases, such as high T_c superconductivity, in intermetallics [1] or cuprates [2–4], and colossal magnetoresistance in manganites [5–8] occur in particular metastable phases reached by driving the material at the edge of a catastrophe. This criticality is reached by tuning a physical variable, such as pressure or charge density, in the proximity of a quantum critical point [9] where several charge, spin, orbital and lattice ordered phases compete, so that in this regime MePhS could show up. In cuprates the quantum criticality is reached by driving a correlated metallic phase (a doped charge transfer Mott insulator) at the edge of an insulating Wigner polaron crystal by changing the chemical pressure [10, 11], involving multi scale phase separation at critical points of structural phase transitions in perovskites [2, 12].

A particular class of quantum phase transitions can be reached by tuning the chemical potential near critical points of the electronic structure that are called electronic topological transitions (ETT) or Lifshitz transitions [14]. At the ETT a phase separation, due to negative compressibility of the electron gas, and the lattice instabilities due to large phonon softening, called Kohn anomalies, could appear [15]. Near

these critical points several phases compete and dynamical quantum fluctuations related to the uncertainty principle can give novel quantum phases [9].

Particular types of ETTs can be realized in materials with particular atomic architectures. For example in a simple two-dimensional (2D) metallic membrane of finite nanoscale thickness N (made of one or few atomic layers), the quantum size effects give a multiband electronic structure made of subbands with different parity determined by the quantization in the thickness direction. Here the tuning of the chemical potential at an ETT (for example at the bottom of a subband) can be done by changing the thickness of the membrane [16]. A second example of material architecture is a three-dimensional (3D) heterostructure at the atomic limit made of a superlattice of first metallic units intercalated by second units with a different electronic structure [17–19]. Its multiband electronic structure shows different subbands and ETT of the type '*opening of a neck*' in only one of the multiple Fermi surfaces [19–25]. The chemical potential can be tuned near an ETT by changing the architecture, the pressure, or charge density.

The superconducting phase in these heterostructures at the atomic limit is described by the BCS theory of multiband systems; for the case of overlapping bands with no hybridization, i.e., spatially separated and with different symmetry, that gives different order parameters (superconducting gaps) in each subband that coexist and form a single macroscopic condensate with a single critical temperature [17–25]. Kondo first pointed out that in multiband superconductivity the interband exchange-like coupling term, that allows the pair exchange between subbands with different gaps, also gives an increase of the critical temperature if it is due to the Coulomb repulsion [26].

Driving the chemical potential very close to one of the ETTs of these heterostructures at the atomic limit the quantum interference between pairing processes shows a resonance called 'shape resonance' [16–22] that is similar to the Feshbach resonance in the many body theory of nuclear and atomic physics [27]. It has also been called a Feshbach shape resonance [23–25]. The high superconducting critical temperature in cuprates [28–33] and diborides [33–35] has been assigned to these resonances.

The key open problem that we want to discuss in this work is that these shape resonances occur in the proximity of the ETT where the crystal is usually unstable being on the verge of a lattice catastrophe. For example it is well known that the lattice of intercalated graphite compounds (IGC) [33] is unstable if the chemical potential is pushed below the top the σ band, therefore there are no IGC materials with holes in the σ band and shape resonance at the ETT could not be reached.

The diboride XB_2 crystals (X = Al, Sc, Ti, Nb, Zr, ...) with hexagonal structure (space group $P6/mmm$) are formed by a heterostructure at the atomic limit made of boron graphene metallic layers intercalated by hcp hexagonal X atomic layers (playing the role of spacers). They have an electronic structure similar to an intercalated graphite compound, where the chemical potential is above the top of the σ band. MgB_2 is a unique diboride, where the chemical potential has been moved below the top of the σ band [36, 37]. By changing the charge density [34] or pressure [38] several ETT in the σ band can be approached. In fact MgB_2 is in the proximity of an ETT of the type '*disruption of a neck*' where the critical temperature is amplified by the shape resonance, giving a relevant interband coupling term [39] that drives the superconducting critical temperature to 40 K, the highest critical temperature between known intermetallics, in agreement with the predictions in [17–19].

In the superconducting ternary $Mg_{1-x}A_xB_2$ intermetallics ($A = Al^{3+}$, Sc^{3+}), $Mg_{1-x}Al_xB_2$ [40–63] and $Mg_{1-x}Sc_xB_2$ [64–66] by changing x we are tuning:

- *the charge transfer* $Q = 3x + 2(1 - x)$, from the boron layers to the X hcp layers;
- *the superlattice period* i.e., the spacing between the boron layers;
- *the chemical pressure* on the boron layer due to the lattice mismatch between the boron and the hcp X layers, controlled by the average ionic radius in the Al/Mg layer, that induces a tensile (compressive) microstrain of the boron (hcp X) monolayers;
- *the quenched disorder* due to the different ionic radii of Mg^{2+} and Al^{3+} ions randomly distributed in the hcp intercalated layers.

$Mg_{1-x}Al_xB_2$ in the range $0 < x < 0.57$, is a clear multiband and multigap (Δ_σ, Δ_π) superconductor [43–46] where the critical temperature is controlled by tuning the position of the chemical potential relative to the critical points of the electronic topological transitions. The σ band is fully occupied in the non-superconducting diboride AlB_2 where only the π band crosses the Fermi level as in intercalated graphite. Replacing aluminum with magnesium injects holes in the boron layers and it moves the chemical potential across the top of the σ band at $E_F = E_A$, in fact at $x = 0.57$ a '*new detached spot*' due to the 3D σ Fermi surface appears, called a type (I) ETT in [23–25]. At $x = 0.3$, $E_F = E_\Gamma$, a type (II) [23–25] Lifshitz electronic topological transition with the '*disruption of a neck*' appears in the corrugated tubular σ Fermi surface. A third, ETT occurs at $x = 0.1$ where the topology of one of the two π bands changes from a 3D open to a 3D closed Fermi surface with the '*disruption of a neck*' as shown in figure 1.

Structural instabilities are expected by tuning the chemical potential near the critical points of the electronic structure since the compressibility of the electron gas becomes negative and phase separation becomes possible in the presence of inhomogeneities. Therefore the presence of quenched disorder in the critical regions can give rise to striking phenomena. The atomic scale local inhomogeneity in these ternary diborides is due to the out-of-plane disorder expected to produce a randomness in potential energy and electron number that randomly moves the chemical potential above or below the ETT critical points. Therefore the out-of-plane disorder plays a key role in controlling the nanoscale phase separation and could be either positive or negative for high T_c superconductivity.

In $Mg_{1-x}Al_xB_2$ the large difference between the ionic radii of Al^{3+} and Mg^{2+} give a disorder that is large enough

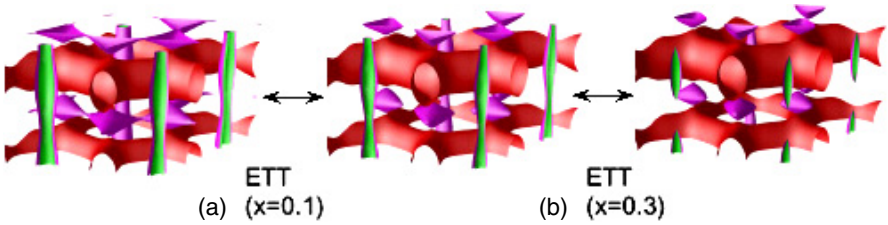

Figure 1. (a) At $x = 0.1$ one of the two π Fermi surfaces undergoes a first electronic topological transition (ETT_1) from an open to a closed 3D Fermi surface with the 'disruption of a neck'; (b) at $x = 0.3$ there is a second ETT_2 where the σ Fermi surface changes from a corrugated tube, with 2D topology, to a closed Fermi surface, with 3D topology (from band structure calculations [35]).

to allow a nanoscale phase separation with metastable phases close to the ETT. It is therefore relevant to compare this system with $Mg_{1-x}Sc_xB_2$ [64–66], where the amplitude of the quenched disorder is much less since the ionic radii of Mg and Sc are very similar. A multiphase behavior has already been reported for $Mg_{1-x}Al_xB_2$ around $0.1 < x < 0.2$ [62] and in $Mg_{1-x}Sc_xB_2$ for $x < 0.12$ [64].

In this paper, we report a detailed study of the lattice structure of the system $Mg_{1-x}Al_xB_2$, going from MgB_2 to AlB_2 through changing the Al content, by high resolution x-ray powder diffraction using synchrotron radiation and micro-Raman spectroscopy in order to study the mesoscopic phase separation.

2. Experimental methods

We have synthesized many polycrystalline samples of $Mg_{1-x}Al_x^{10}B_2$ (with the boron pure isotope ^{10}B) in a wide range of concentration ($0 < x < 0.57$) by direct reaction of the elemental magnesium, aluminum, and boron (99% purity). The starting material powders (325 mesh) were mixed in the stoichiometric ratio and pressed into a pellet. The pellet was enclosed in tantalum crucible and sealed by arc welding under an argon atmosphere into the glove box where humidity and oxygen levels were continuously monitored so that $[H_2O] < 0.1$ ppm and $[O_2] < 1$ ppm. The arc welding was localized on the top of the crucible and the sample was not exposed to high temperature during the welding process. The arc sealing of the crucibles does not allow Mg and Al to diffuse out of the crucible during the reaction. The Ta crucibles enclosed in a glass ampoule filled with argon were then heated for 1 h at 800 °C and 2 h at 950 °C in the oven and then cooled rapidly to room temperature.

In order to check the mixing process resulting from the same starting powder mixture, three different pellets with the same nominal Al concentration were prepared. Several different pieces taken from the top, the bottom, the inner and the outer part of the same pellet were analyzed to look for any Al gradient or extrinsic inhomogeneity.

The characterization of the samples was done using a scanning electron microscope (SEM) LEO1450VP (Assing) equipped for the energy dispersion spectroscopy (EDS) with an INCA300. A representative SEM micrograph on the sample with $x = 0.28$ is shown in figure 2, where it is possible to see a typical well faceted hexagonal microcrystal of about 1–2 μm that is the basic component of our powder samples.

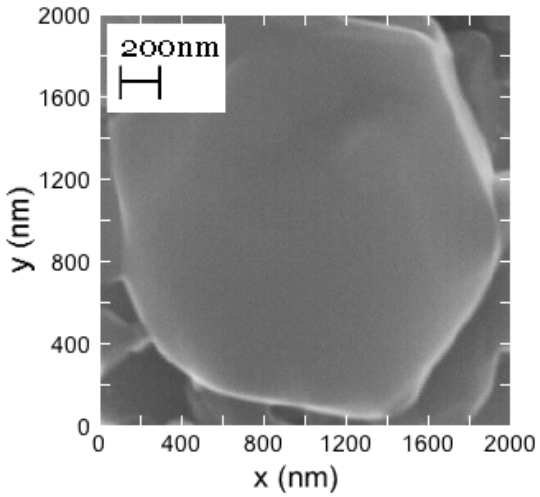

Figure 2. SEM micrographs of a microcrystal exhibiting a excellent hexagonal faceted shape of the ternary intermetallic system $Mg_{1-x}Al_xB_2$ with $x = 0.28$ where the chemical potential is very close to the 2D/3D ETT with the 'disruption of a neck' in the σ band and in the proximity of a large structural instability.

These microcrystals are observed in all samples with different Al content.

The phase purity of the samples was checked by electron dispersion spectroscopy (EDS). The actual Al content was checked with at least 20 different measurements on different grains of each sample. The results show that the actual Al/Mg ratio in each crystal is very close to the nominal content within the experimental error.

The diffraction experiment was carried out at the high resolution powder diffraction beam line ID31 of the European Synchrotron Radiation Facility (ESRF) in Grenoble. The samples were reduced to a fine dust using a pestle and a mortar and sealed in 1.0 mm diameter capillaries made of a glass (glass no. 5), whose contribution to the profile background (i.e. Compton incoherent scattering) is very low. The diffraction profiles, using an incident x-ray wavelength $\lambda = 0.500\,15$ Å and nine Si(111) analyzer crystals, were collected as a function of 2Θ, where Θ is the Bragg angle, in order to get the range of the momentum transfer $1\ \text{Å}^{-1} < q < 9\ \text{Å}^{-1}$. About 150 high resolution diffraction profiles were collected at room temperature.

The diffraction patterns were analyzed by Rietveld refinement using the GSAS program (General Structural

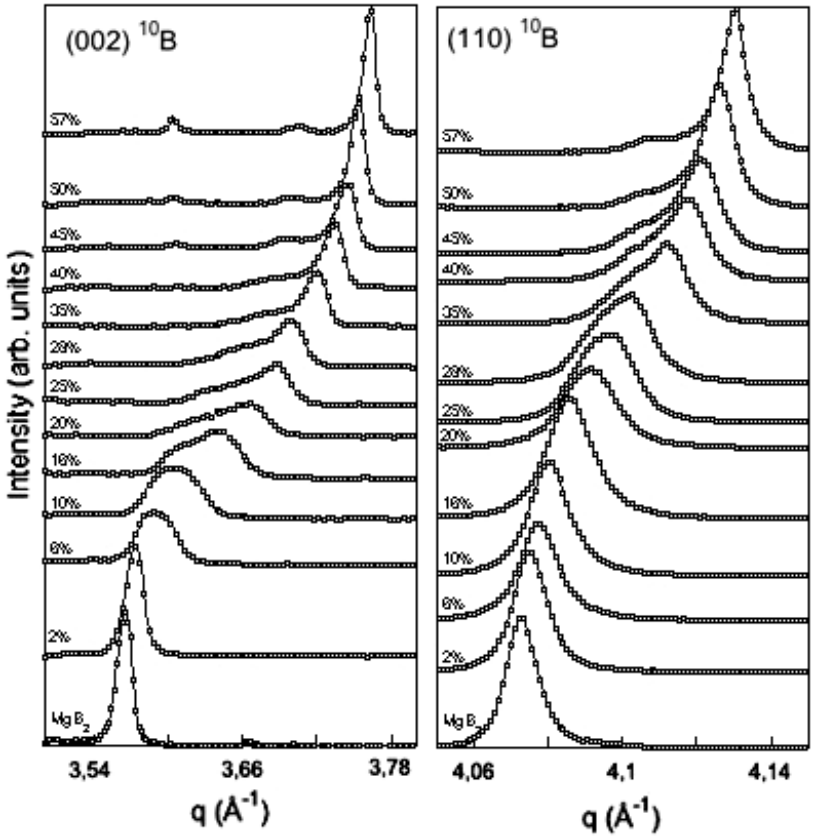

Figure 3. Evolution of the (110) and (002) x-ray diffraction reflection peaks as a function of Al content.

Analysis Software). The reflections are indexed according to the hexagonal $P6/mmm$ structure. No trace of MgB_4 or MgB_7 were found although a very small impurity peak due to MgO was found in a few samples. The high quality powder diffraction data show a small instrumental contribution to the diffraction line width due to the highly parallel beam optics geometry at the ID31.

As Rietveld fits need a starting model, a preliminary study of the raw data was made in order to make a correct fit. This study was performed on the (002) (i.e. the c-axis) and (110) (i.e. the a-axis) diffraction lines.

The Raman spectra were measured at NTUA in Athens in the back-scattering geometry, using a T64000 Jobin–Yvon triple spectrometer with a charge-coupled device camera. The range of Raman shift explored was between 50 and 1200 cm^{-1}. The 488.0 and 531.1 nm laser line was focused on 1–2 μm large crystallites and the power was kept below 0.1 mW to avoid heating by the beam. Several measurements on several single micro-crystallites were performed for each sample.

3. Results and discussion

3.1. High resolution powder diffraction

The general behavior of the structure of the $Mg_{1-x}Al_xB_2$ samples as a function of Al content can be seen in figure 3, where we report the (002) and (110) XRD reflections, representing the inter-plane and intra-plane evolution, as a function of the momentum transfer $q = 4\pi \sin\theta/\lambda$. The (002) and the (110) reflection peaks shift to high q values with the Al content but the variation is much larger along the c direction than in the ab plane, due to the difference in bond strengths: the covalent B–B bonds in the basal plane are stronger than the Mg–B ionic bonds. Both the (002) and (110) reflections broaden with an increase of the Al content due to the quenched disorder for the different Mg and Al ionic radii. The (002) reflection peak splits for $x > 0.075$ so that between 7.5% and 28% of Al content the system shows a clear phase separation along the c axis that evolves as a function of x in agreement with the results obtained by Slusky *et al* [62].

The profiles of the (002) x-ray reflection in figure 3 shows the following features:

(i) at $x = 1$, AlB_2, the profile of the (002) reflection is sharper than for $x = 0$, MgB_2. Therefore the line width of the $x = 0$ samples show a relevant disorder assigned to magnesium vacancies that rapidly disappear with finite Al content;

(ii) in the range $0 < x < 0.07$ the profile of the (002) reflection becomes wider with increasing Al content indicating increasing disorder due to the different ionic radii of Al and Mg, but there is no second well resolved peak;

(iii) in the range $0.07 \leqslant x < 0.3$ two peaks are well resolved indicating two different phases: the first one with a shorter c-axis, called 'relaxed' phase (R) and a second phase with

longer c axis called 'tense' phase (T), the two phases have nearly the same weight for $x = 0.10$;

(iv) by increasing x the profile of the (002) reflection of the R (T) phase gets sharper and stronger (broader and weaker) so that for $x > 0.3$ the probability of the phase with longer c axis becomes negligible;

(v) while the peak of the 'tense' phase shows a nearly linear shift with Al content (Vegard's law) the peak of the 'relaxed' phase shows a large deviation from Vegard's law.

The profiles of the (110) x-ray reflection in figure 3 show the following features:

(i) in the range $0 < x < 0.25$ the profile of the (110) reflection becomes wider with increasing Al content indicating increasing disorder due to the different ionic radii of Al and Mg, but there is no second well resolved peak;

(ii) in the range $0.2 < x < 0.5$ two peaks are well resolved indicating two different phases the first one with a shorter a-axis, called 'relaxed' phase (R) and a second phase with longer a axis called 'tense' phase (T), the two phases have nearly the same weight for $x = 0.30$;

(iii) while the peak of the 'relaxed' phase shows a nearly linear shift with Al content (Vegard's law) the peak of the 'tense' phase shows a large deviation from Vegard's law.

The crystalline structure was extracted by Rietveld analysis of the XRD data. A single phase model was used for the low Al content ($0 < x < 0.05$) and for the high Al content ($x \geqslant 0.54$) while a two phase model was used in the range $0.05 \leqslant x < 0.54$.

In figure 4 the deviation from Vegard's law of the a-axis and the c-axis of the two phases (labeled R for the 'relaxed' phase and T for the 'tense' phase) as a function of the Al content x are plotted. The contraction of the lattice parameters for a random solid solution are expected to follow the average ionic radius $r(x) = 160 - 17x$ pm (in fact $r(Mg^{+2}) = 160$ pm and $r(Al^{+3}) = 143$ pm). Vegard's law for the a-axis is given by $a(x) = 3.085\,09–0.078\,62x$ and for the c axis by $c(x) = 3.525\,613–0.271\,553x$.

The a-axis (c-axis) lattice parameter of the 'relaxed' ('tense') phase are close to linear Vegard's law but show a nonlinear variation with x. The c-axis (a-axis) lattice parameter of the 'relaxed' ('tense') phase show strong deviations from linear Vegard's law with variable x. The large deviations from Vegard's law show that the atomic substitutions induce an anisotropic chemical pressure that is nonlinearly dependent on the average ionic size.

In figure 5 the splitting between the two phases along the c-axis (Δc) and the a-axis (Δa) is plotted versus x. The splitting of the c-axis shows a rapid increase around $x = 0.10$, i.e. at the 'disruption of a neck' in the π-band here called ETT_1, shown in figure 1. The splitting of the a-axis is observed at $x = 0.30$ where the 2D/3D ETT_2 i.e., the 'disruption of a neck' in the σ-band shown in figure 1 is expected. Therefore these results show that the phase separation in the proximity of the '*disruption of a neck*' in the π-band (σ-band) at ETT_1 (at ETT_2) gives a 'relaxed' phase (R) and a 'tense' phase (T) characterized by a short and a long c-axis (a-axis).

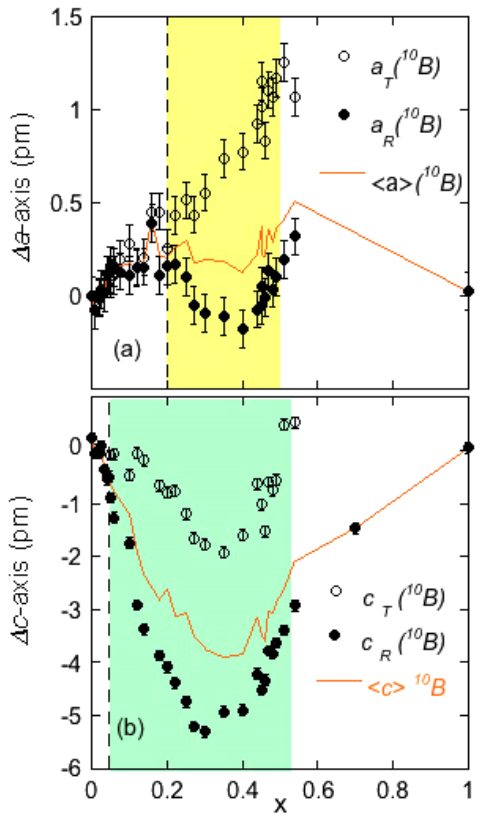

Figure 4. The deviation from the expected linear variation (Vegard's law) of the lattice parameter $a(x)$ and $c(x)$ from AlB_2 ($x = 0$) to MgB_2 ($x = 1$) of the two coexisting phases the first 'relaxed' (R filled circles) and the second 'tense' phase (R open circles).

From the difference between the unit cell volume of the 'relaxed' and 'tense' phase it is possible to measure the effective variation Δx of Al content x between the two phases reported in panel (c) of figure 5, which is a measure of the difference between the two phases of the charge transfer from the boron to the (Mg/Al) layer.

The two phases can be characterized by the plot of the ratio c/a as a function of the normalized unit cell volume shown in figure 6. The ratio c/a is an important physical parameter related to the chemical anisotropic pressure due to the internal mismatch between the boron layers and the (Mg/Al) layers. In fact the tensile microstrain in the boron layer and the opposite compressive microstrain in the Al/Mg layer can be estimated by considering that where c/a is 1.075, the two lattices are well tuned, and therefore the microstrain is zero. The tensile microstrain can be defined as $\eta = (0.93\text{c/a} - 1)$ and it is shown on the scale at the left side of figure 6. The effective Al content x, measuring the charge transfer, extracted from the measure of the volume of the unit cell in each phase is shown in the x axis in the upper part of figure 6. The results show that the 'tense' phase (with a larger c/a ratio or larger tensile microstrain) has more holes per boron ion (hole rich) than the 'relaxed' phase (hole poor). The effective aluminum concentration x in the 'tense' phase is always smaller than 0.5. Therefore in the samples with the aluminum content x larger than 0.5, the phase separation occurs between two phases

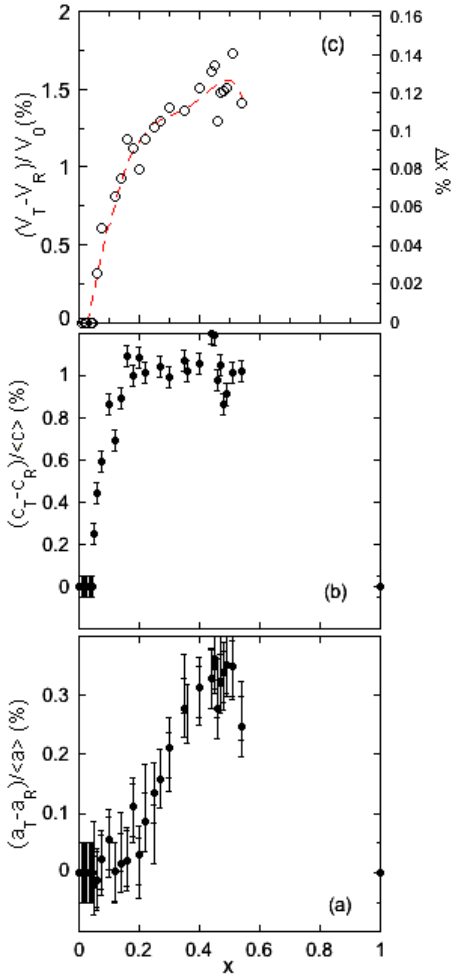

Figure 5. Evolution of the splitting of the lattice parameters $a(x)$, $b(x)$ and the volume $V(x)$ between the 'tense' (T) and the 'relaxed' (R) phase as a function of Al content x. Panel (c) shows also the effective variation Δx of Al content x between the 'relaxed' and 'tense' phase measured from the difference between the unit cell volume.

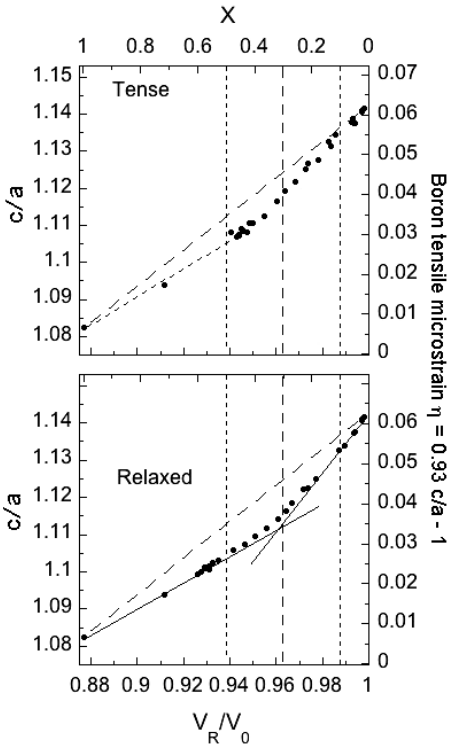

Figure 6. Evolution of the c/a ratio for the 'relaxed' (R), lower panel, and the 'tense' phase (T) upper panel, as a function of the volume of the 'relaxed' and 'tense' phase normalized to the unit cell volume of MgB_2. The upper x axis gives the effective aluminum content in each phase measured from the unit cell volume of the corresponding phase. The chemical anisotropic pressure is measured by the internal boron tensile microstrain that is given in the y-axis on the left side of the plot.

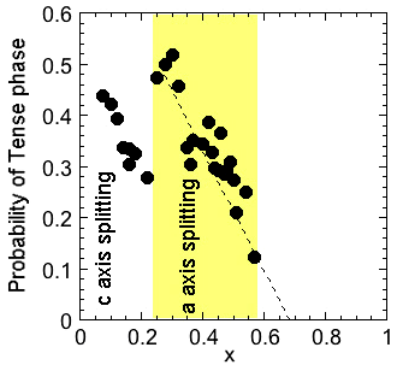

Figure 7. Evolution of the probability of the 'tense' phases characterized by the c-axis splitting ($0.07 < x < 0.25$) and the a-axis splitting ($0.25 < x < 0.57$) as a function of Al content.

with effective Al content smaller ('tense') or larger ('relaxed') than 0.5.

In figure 7 the relative weight of the 'tense' phases extracted by Rietveld analysis is plotted as a function of x. The data show that at the two onsets of the phase separation, $x_1 \approx 0.1$ and $x_2 \approx 0.3$, the two competing phases R and T have nearly equivalent probability and beyond this point the relative weight of the 'tense' phase decreases rapidly. With increasing Al content x the system becomes disordered due to the variance of the ionic radii of Al and Mg ions which is expected to induce a disorder due to a tensile expansion in the domains around the large Mg ions and the compression or relaxation in the domains around Al ions. Diborides are layered materials where the layers can be pulled apart without much effort but the layers themselves are quite hard, therefore the local lattice strain is also expected to be anisotropic. The broadening is expected to be larger in the squishy direction (c-axis) and smaller in the layer direction. The quantitative measure of the anisotropic lattice disorder has been extracted by Rietveld analysis of the XRD data giving the strain variance defined as [67]:

$$\sigma^2(M_{hkl}) = \sum_{HKL} S_{HKL} h^H k^K l^L, \qquad H + K + L = 4$$

that for the case of the hexagonal lattice $6/mmm$ is given by:

$$\Gamma_S^2 = S_{400}(h^4 + k^4 + 3h^2k^2 + 2h^3k + 2hk^3) + S_{004}l^4 + 3S_{202}(h^2l^2 + k^2l^2 + hkl^2).$$

The values S_{400} and S_{004} are reported in figure 8 as a function of Al content for the first 'relaxed' (R) phase and

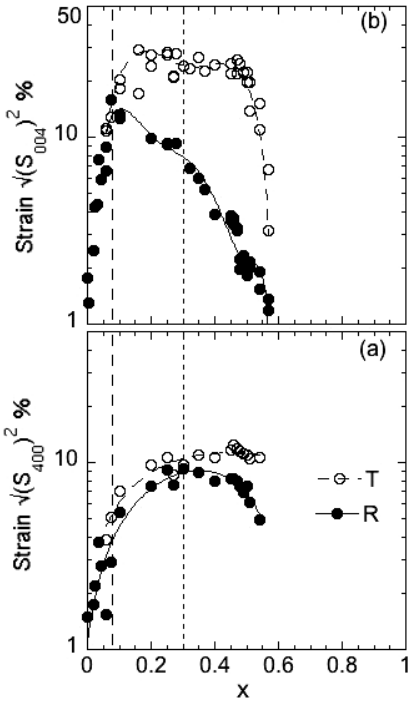

Figure 8. The strain due to the lattice disorder extracted from Rietveld analysis in the *ab* plane (S_{400}) and the in the *c*-axis direction (S_{004}) as a function of Al content for the first 'relaxed' (R, filled symbols) phase and the second 'tense' (T, open symbol) phase.

the second 'tense' (T) phase. The disorder rapidly increases in the *c*-axis direction (more than in the *a*-axis direction) where S_{004} reaches 15% at the small Al content x of about 0.07 where we observe the onset of phase separation between the 'tense' and the 'relaxed' phase. The disorder continues to increase with Al content reaching saturation at $x = 0.4$ in the 'tense' phase as expected. On the contrary the disorder in the 'relaxed' phase R decreases with increasing Al content beyond the critical point for the phase separation recovering the low disorder as in magnesium diboride at $x = 0.5$. The disorder in the boron plane direction, measured by S_{400}, continues to increase up to $x = 0.3$ where the second phase separation between the *in-plane 'tense'* and the *in-plane 'relaxed'* phase occurs. Beyond the critical point for the phase separation the disorder of the 'relaxed' phase decreases from $x = 0.3$ to 0.5. These results show that the phase separation at the critical points, $x_1 \approx 0.1$ and $x_2 \approx 0.3$, occurs between two phases with a large local lattice distortion. By comparing the phase separation in samples with Al substitutions with the similar case of Sc substitutions [64–66], we can conclude that, in Al doped samples we can drive the system very close to the ETT critical points because of local disorder that allows the mesoscopic phase separation, while in the Sc doped materials with lower disorder the system shows the macroscopic phase separation.

The mesoscopic phase separation in our samples can be quantified by extracting the size of the crystalline ordered domains for the 'tense' and the 'relaxed' phases that are plotted in figure 9. The effective crystalline domain size of the T and R phase is much smaller than the size of our microcrystals,

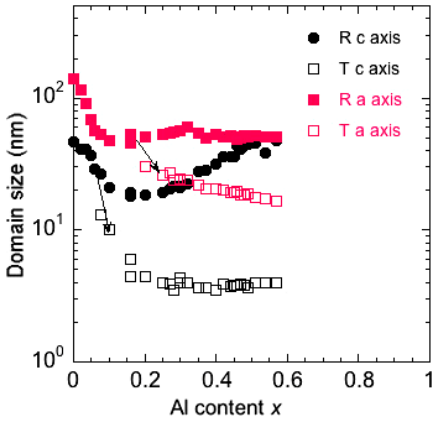

Figure 9. The size of the crystalline domains of the first 'relaxed' (R, filled symbols) phase and the second 'tense' (T, open symbol) phase in the *c* axis direction and in the ab plane direction as a function of Al content.

showing that the mesoscopic phase separation occurs within the same microcrystal. The domain size is clearly smaller in the *c* axis than in the *a*-axis direction, and much smaller for the 'tense' phase where it reaches the mesoscopic domain size of 20 nm in the planar direction and 5 nm in the *c*-axis direction.

3.2. Micro-Raman spectroscopy

In the simple hexagonal structure of $Mg_{1-x}Al_xB_2$ four zone-center optical modes are expected: the E_{2g} Raman active mode, the Raman silent B_{1g} mode and the infrared active E_{1u} and A_{2u} modes. The doubly degenerate E_{2g} modes are due to in-plane stretching modes of the boron atoms, the Mg and B planes vibrate in opposite directions along the x (or y) axis in the E_{1u} mode, and the A_{2u} and B_{1g} singly degenerate modes involve vibrations along the c axis. In the B_{1g} mode the boron atoms move in opposite directions while the Mg is stationary, in the A_{2u} mode the Mg and B planes move in opposite directions along c. An analysis of phonon dispersion in MgB_2 reveals the following energies for the modes.

The micro-Raman spectra after background subtraction are reported in figure 10 for the samples with Al content $0 < x < 0.57$. The A_{2u} and E_{1u} phonon modes are weak and show only negligible shift with Al content.

The in-plane boron vibration with E_{2g} symmetry can be easily identified the Raman spectrum of AlB_2 where it is a single dominant narrow peak. In the data we can easily identify the forbidden B_{1g} phonon mode activated by the lattice disorder that evolves as a function of Al content in $Mg_{1-x}Al_xB_2$, reaching a maximum at about 30% aluminum content in good agreement with previous Raman studies [48, 50] on this ternary system.

The analysis of the Raman spectra was performed by fitting the E_{2g} and B_{1g} phonon modes as a function of Al content with a three Gaussian curves model. In figure 11 we report the evolution of the best-fit values of frequency and the full width of the Raman signals.

The B_{1g} does not change abruptly as a function of x, its frequency reported in figure 11 panel (a) increases almost

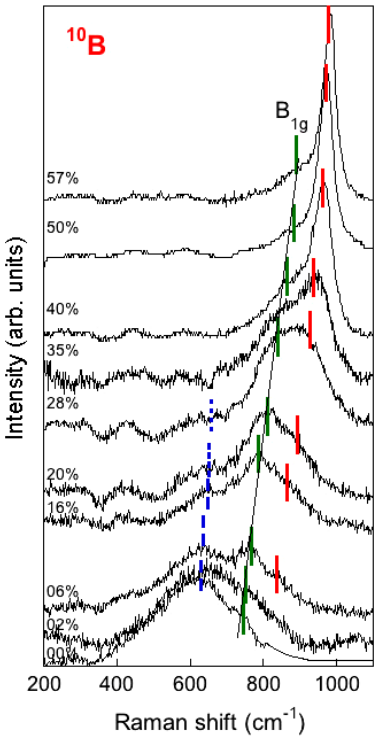

Figure 10. Raman spectra of $Mg_{1-x}Al_x^{10}B_2$ ($0.06 < x < 0.57$) showing the evolution with Al concentration of the forbidden B_{1g} mode allowed by the quenched disorder, and the split of the E_{2g} mode into a soft (dashed blue) and hard (solid red) component.

linearly with increasing Al content and its full width remains around 40 cm^{-1}. The intensity of this line shows a rapid increase from $x = 0$ to 0.3, with a maximum around 30% of Al content, as plotted in figure 12, panel (b). The intensity of this line is clearly related to the lattice disorder measured in this work and reported in figure 8. The comparison shows that the B_{1g} becomes Raman active because of the in-plane lattice disorder measured by S_{400}.

The E_{2g} phonon mode undergoes a substantial variation in terms of frequency and width as a function of Al content. The high statistics and resolution allows us to detect the splitting of the E_{2g} phonon mode into soft and hard components between 6% and 28% of Al content. The frequencies of the two E_{2g} phonon modes are reported in figure 11 panel (a) and their full width in panel (b). The relative intensity of the two modes is plotted in panel (a) of figure 12. In the range $6 < x < 0.3$ both the two E_{2g} contributions are wide.

There is a clear agreement between the results obtained by high resolution x-ray diffraction and by micro-Raman measurements. First of all, both from Raman and XRD measurements, it is evident that the chemical substitution increases the structural disorder in the system, with a maximum around $x = 0.30$. In fact, the lattice strain due to the variance between the Al–Mg atomic radii shows a maximum around 30% of Al content and at the same time, the intensity of the silent B_{1g} mode, activated by disorder, increases with increasing Al content up to 30% and then decreases again.

The energy asymmetry in the E_{2g} mode detectable for $x > 0.28$ could be associated with the lattice in-plane phase separation observed by x-ray diffraction.

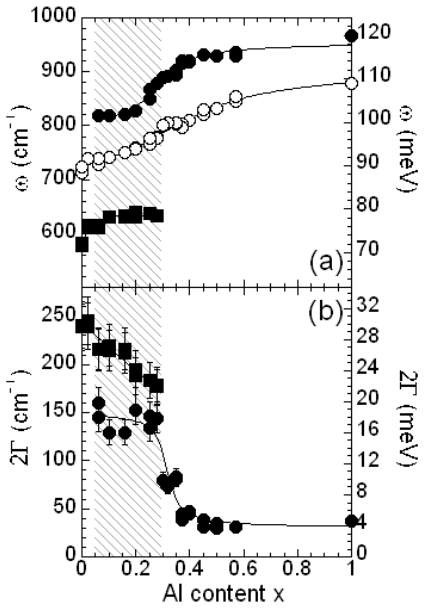

Figure 11. Panel (a) the energy of the E_{2g} mode (filled squares and circles) and the B_{1g} mode (empty circles) as a function of Al content from the analysis of the Raman spectra of $Mg_{1-x}Al_xB_2$ samples. The filled circles and squares represent the hard and soft E_{2g}, respectively. Panel (b) the full width of the soft (filled squares) and hard (filled circles) E_{2g} mode.

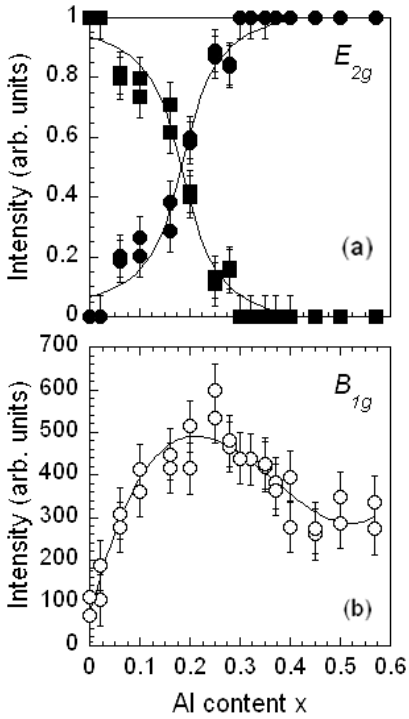

Figure 12. Evolution of the intensity of the hard (filled squares) and soft (filled circles) E_{2g}, panel (a), and the intensity of the B_{1g} (open circles) phonon mode, panel (b), as a function of Al content.

The E_{2g} phonon splitting agrees well with the results of Goncharov *et al* [38] since the chemical pressure varied by changing the Al content is an anisotropic pressure. In fact the results in [38] reported the variation of the Raman spectra and

x-ray diffraction applying an hydrostatic and a non-hydrostatic pressure on MgB_2. They found a splitting of the Raman spectra and, at the same time, a splitting of the (002) reflection peak using anisotropic pressure which did not occur when applying an isotropic pressure.

4. Conclusions

In conclusion we have investigated the phase separation in the ternary superconducting $Mg_{1-x}Al_xB_2$ system near the critical points of the electronic structure by high resolution x-ray powder diffraction and micro-Raman measurements.

Between $x = 0.06$ and 0.28 we detect a splitting in the (002) reflection peak, while the splitting of the (110) reflection is not resolvable. In the same range of concentrations the contribution to the Raman spectra of the E_{2g} mode splits. This first phase separation occurs around 10% of Al content where a π band changes topology. We found that this phase separation is related to the anisotropic pressure due to the chemical substitution and quenched lattice disorder.

A second phase separation occurs after 28% of Al content, near the II type ETT, where the phase separation involves only the in-plane direction and results in anisotropy of the E_{2g} Raman peak.

We have obtained indications that electronic topological transitions could drive the system at the verge of a catastrophe, where structural, electronic and phonon properties change dramatically. Here the mesoscopic phase separation occurs, as in highly correlated electronic systems, near the critical point of the electronic structure and the quenched disorder plays a key role near a bicritical region [6]. In fact we have shown that at a random potential related to the quenched disorder the two phases, R and T, coexist at various length scales. Therefore the phase separation that also occurs in this system could be explained in terms of the critical points of the electronic structure.

Acknowledgments

We thank Matteo Filippi for experimental help and discussions. We acknowledge financial support from European STREP project 517039 'Controlling Mesoscopic Phase Separation' (COMEPHS) (2005).

References

[1] White R W and Geballe T H 1979 *Long Range Order in Solids* ed H Ehrenreich, F Seitz and D Turnbull (New York: Academic)

[2] Müller K A and Berlinger W 1968 Characteristic structural phase transition in Perovskite-type compounds *Phys. Rev. Lett.* **21** 814–7
Müller K A and Berlinger W 1971 Static critical exponents at structural phase transitions *Phys. Rev. Lett.* **26** 13–6
Müller K A and Burkard H 1979 $SrTiO_3$: an intrinsic quantum paraelectric below 4 K *Phys. Rev.* B **19** 3593–602
Thomas H and Müller K A 1968 Structural phase transitions in perovskite-type crystals *Phys. Rev. Lett.* **21** 1256–9
Müller K A 1974 Critical phenomena near structural phase transitions studied by EPR *Ferroelectrics* **7** 17–21
Bednorz J G and Müller K A 1986 Possible high T_c superconductivity in the BaLaCuO system *Z. Phys.* B **64** 189–93
Georg Bednorz J and Alex Müller K 1988 Perovskite-type oxides-the new approach to high-T_c superconductivity *Rev. Mod. Phys.* **60** 585–600

[3] Kivelson S A, Aeppli G and Emery V J 2001 *Proc. Natl Acad. Sci.* **98** 11903–7
Kivelson S A 2006 *Nat. Mater.* **5** 343
Mohottala H E *et al* 2006 *Nat. Mater.* **5** 377–82

[4] Kusmartsev F V, Di Castro D, Bianconi G and Bianconi A 2000 Transformation of strings into an inhomogeneous phase of stripes and itinerant carriers *Phys. Lett.* A **275** 118

[5] Dagotto E 2005 Complexity in strongly correlated electronic *Syst. Sci.* **309** 257–62

[6] Tokura Y 2006 *Rep. Prog. Phys.* **69** 797–851

[7] Mathur N and Littlewood P 2003 *Phys. Today* **56** 25
Calderon M J, Milward G C and Littlewood P B 2005 *Nature* **433** 607

[8] Renner Ch, Aeppli G, Kim B-G, Soh Y-A and Cheong S-W 2002 Atomic-scale images of charge ordering in a mixed valence manganite *Nature* **416** 518–21

[9] Sachdev S 1999 *Quantum Phase Transitions* (Cambridge: Cambridge University Press)
Sachdev S 2003 *Rev. Mod. Phys.* **75** 913

[10] Bianconi A, Agrestini S, Bianconi G, Di Castro D and Saini N L 2001 A quantum phase transition driven by the electron lattice interaction gives high T_c superconductivity *J. Alloys Compounds* **317/318** 537–41

[11] Di Castro D, Bianconi G, Colapietro M, Pifferi A, Saini N L, Agrestini S and Bianconi A 2000 Evidence for the strain critical point in high T_c superconductors *Eur. Phys. J.* B **18** 617

[12] Agrestini S, Saini N L, Bianconi G and Bianconi A 2003 The strain of CuO_2 lattice: the second variable for the phase diagram of cuprate perovskites *J. Phys. A: Math. Gen.* **36** 9133–42
Büchner B *et al* 1993 Competition between structural and superconducting transition in (LaNd)–Sr–Cu–O *Europhys. Lett.* **21** 953–8
Alex Müller K, Dorner B and Thomas H 1981 *Structural Phase Transitions* (*Springer Statistical Physics*) (Berlin: Springer) ISBN 0387103295
Fujimoto Minoru 2004 *The Physics of Structural Phase Transitions* (*Springer Lattice Dynamics*) (Berlin: Springer) ISBN 0387407162

[13] Aeppli G *et al* 1997 *Science* **278** 1432–5

[14] Lifshitz I M 1960 *Sov. Phys.—JEPT* **11** 1130

[15] Flattè Michael E 1994 Kohn anomalies in superconductors *Phys. Rev.* B **50** 1190
Grüner G 2000 *Density Waves in Solids* (Cambridge, MA: Perseus)
Olijnyk H, Jephcoat A P, Novikov D L and Christensen N E 2000 *Phys. Rev.* B **62** 5508

[16] Blatt J M and Thompson C J 1963 *Phys. Rev. Lett.* **10** 332
Thompson C J and Blatt J M 1963 *Phys. Lett.* **5** 6
Blatt J M 1964 *Theory of Superconductivity* (New York: Academic)

[17] Bianconi A 1996 Process of increasing the critical temperature T_c of a bulk superconductor by making metal heterostructures at the atomic limit *US Patent Specification* 6265019; see http://www.google.com/patents?id=WJcHAAAAEBAJ&dq=patent:6265019

[18] Bianconi A 1997 High T_c superconductors made by metal heterostuctures at the atomic limit *European Patent Specification* 0733271; see http://www.wipo.int/pctdb/en/wo.jsp?wo=1995016281

[19] Bianconi A 1994 On the possibility of new high T_c superconductors by producing metal heterostructures as in cuprate Perovskites *Solid State Commun.* **89** 933

[20] Perali A, Bianconi A, Lanzara A and Saini N L 1996 The gap amplification at a shape resonance in a superlattice of quantum stripes: a mechanism for high T_c *Solid State Commun.* **100** 181–6

[21] Bianconi A, Valletta A, Perali A and Saini N L 1997 High T_c superconductivity in a superlattice of quantum stripes *Solid State Commun.* **102** 369–74

[22] Bianconi A, Valletta A, Perali A and Saini N L 1998 Superconductivity of a striped phase at the atomic limit *Physica* C **296** 269–80

[23] Bianconi A 2005 Feshbach shape resonance in multiband superconductivity in heterostructures *J. Supercond.* **18** 25–36

[24] Bianconi A 2006 Feshbach shape resonance for high T_c pairing in superlattices of quantum stripes and quantum wells *Iran. J. Phys. Res.* **6** 139–47

[25] Bianconi A 2006 The Feshbach shape resonance for high T_c superconductivity in superlattices of nanotubes *Phys. Status Solidi* a **203** 2950–5

[26] Kondo J 1963 *Prog. Theor. Phys.* **29** 1 see http:/7www.superstripes.com/

[27] Romans M W J, Duine R A, Sachdev S and Stoof H T C 2004 Quantum phase transition in an atomic Bose gas with a Feshbach resonance *Phys. Rev. Lett.* **93** 020405
Dickerscheid D B M, Al Khawaja U, van Oosten D and Stoof H T C 2005 Feshbach resonances in an optical lattice *Phys. Rev.* A **71** 043604 and references therein

[28] Bianconi A, Saini N L, Rossetti T, Lanzara A, Perali A and Missori M 1996 Stripe structure in the CuO_2 plane of perovskite superconductors *Phys. Rev.* B **54** 12018–21

[29] Bianconi A, Lusignoli M, Saini N L, Bordet P, Kvick Å and Radaelli P G 1996 Stripe structure of the CuO_2 plane in $Bi_2Sr_2CaCu_2O_8$ by anomalous x-ray diffraction *Phys. Rev.* B **54** 4310

[30] Bianconi A, Saini N L, Lanzara A, Missori M, Rossetti T, Oyanagi H, Yamaguchi H, Oka K and Ito T 1996 Determination of the local lattice distortions in the CuO_2 plane of $La_{1.85}Sr_{0.15}CuO_4$ *Phys. Rev. Lett.* **76** 3412–5

[31] Saini N L, Lanzara A, Bianconi A, Oyanagi H, Yamaguchi H, Ota K and Ito T 1996 Temperature dependent Cu–O distribution function of the superconducting CuO_2 plane *Physica* C **268** 121–7

[32] Di Castro D, Colapietro M and Bianconi G 2000 Metallic stripes in oxygen doped La_2CuO_4 *Int. J. Mod. Phys.* B **14** 3438

[33] Bianconi A 2006 Multiband superconductivity in high T_c cuprates and diborides *J. Phys. Chem. Solids* **67** 566–9

[34] Bianconi A, Di Castro D, Agrestini S, Campi G, Saini N L, Saccone A, De Negri S and Giovannini M 2001 A superconductor made by a metal heterostructure at the atomic limit tuned at the 'shape resonance': MgB_2 *J. Phys.: Condens. Matter* **13** 7383–90

[35] Agrestini S, Di Castro D, Sansone M, Saini N L, Saccone A, De Negri S, Giovannini M, Colapietro M and Bianconi A 2001 High T_c superconductivity in a critical range of micro-strain and charge density in diborides *J. Phys.: Condens. Matter* **13** 11689–95

[36] An J M and Pickett W E 2001 Superconductivity of MgB_2: covalent bonds driven metallic *Phys. Rev. Lett.* **86** 4366

[37] Mazin I I and Antropov V P 2003 *Physica* C **385** 49–65 and references cited therein

[38] Goncharov A F and Struzhkin V V 2003 Pressure dependence of the Raman spectrum, lattice parameters and superconducting critical temperature of MgB_2: evidence for pressure-driven phonon-assisted electronic topological transition *Physica* C **385** 117

[39] Choi H J, Roundy D, Sun H, Cohen M L and Louie Steven G 2004 Reply to comment on 'first-principles calculation of the superconducting transition in MgB_2 within the anisotropic Eliashberg formalism' *Phys. Rev.* B **69** 056502

[40] Bianconi A *et al* 2002 Scaling of the critical temperature with the Fermi temperature in diborides *Phys. Rev.* B **65** 174515

[41] Bussmann-Holder A and Bianconi A 2003 Raising the diboride superconductor transition temperature using quantum interference effects *Phys. Rev.* B **67** 132509

[42] Ummarino G A, Gonnelli R S, Massidda S and Bianconi A 2004 Two-band Eliashberg equations and the experimental T_c of the diboride $Mg_{1-x}Al_xB_2$ *Physica* C **407** 121

[43] Samuely P, Szabo' P, Canfield P C and Bud'ko S L 2005 Comment on band filling and interband scattering effects in MgB_2: carbon versus aluminium doping *Phys. Rev. Lett.* **95** 099701

[44] Cooley L D, Zambano A J, Moodenbaugh A R, Klie R F, Zheng J-C and Zhu Y 2005 Inversion of two-band superconductivity at the critical electron doping of (Mg; Al)B_2 *Phys. Rev. Lett.* **95** 267002

[45] Kortus J, Dolgov O V, Kremer R K and Golubov A A 2005 Band filling and interband scattering effects in MgB_2: carbon versus aluminum doping *Phys. Rev. Lett.* **94** 027002

[46] Gonnelli R S, Daghero D, Ummarino G A, Tortello M, Delaude D, Stepanov V A and Karpinski J 2007 Point-contact Andreev-reflection spectroscopy in MgB_2: the role of substitutions *Physica* C **456** 134

[47] Klie R F, Zheng J C, Zhu Y, Zambano A J and Cooley L D 2006 Electron doping in MgB_2 studied by electron energy-loss spectroscopy *Phys. Rev.* B **73** 014513

[48] Di Castro D *et al* 2002 The amplification of the superconducting T_c by combined effect of tuning of the Fermi level and the tensile micro-strain in $Al_{1-x}Mg_xB_2$ *Europhys. Lett.* **58** 278

[49] Postorino P, Congeduti A, Dore P, Nucara A, Bianconi A, Di Castro D, De Negri S and Saccone A 2001 Effect of the Al content on the optical phonon spectrum in $Mg_{1-x}Al_xB_2$ *Phys. Rev.* B **65** 020507(R)

[50] Renker B, Bohnen K B, Heid R, Ernst D, Schober H, Koza M, Adelmann P, Schweiss P and Wolf T 2002 Strong renormalization of phonon frequencies in $Mg_{1-x}Al_xB_2$ *Phys. Rev. Lett.* **88** 067001

[51] Profeta G, Continenza A and Massidda S 2003 *Phys. Rev.* B **68** 144508

[52] Zhang P, Louie S G and Cohen M L 2005 *Phys. Rev. Lett.* **94** 225502

[53] Xu G J, Grivel J C, Abrahamsen A B, Chen X P and Andersen N H 2003 Structure and superconductivity of double-doped $Mg_{1-x}(Al_{0.5}Li_{0.5})_xB_2$ *Physica* C **399** 8–14

[54] Monni M *et al* 2005 Codoped $Mg_{1-x}(AlLi)_xB_2$ compounds: a key system to probe the effect of the charge doping and inter-band scattering arXiv:cond-mat/050616

[55] Luo H, Li C M, Luo H M and Ding S Y 2002 Study of Al doping effect on superconductivity of $Mg_{1-x}Al_xB_2$ *J. Appl. Phys.* **91** 7122–4

[56] Xiang J Y, Zheng D N, Li J Q, Li S L, Wen H H and Zhao Z X 2003 Effects of Al doping on the superconducting and structural properties of MgB_2 *Physica* C **386** 611–5

[57] Putti M, Ferdeghini C, Monni M, Pallecchi I, Tarantini C, Manfrinetti P, Palenzona A, Daghero D, Gonnelli R S and Stepanov V A 2005 Critical field of Al-doped MgB_2 samples: correlation with the suppression of the s-band gap *Phys. Rev.* B **71** 14405

[58] Birajdar B, Wenzel T, Manfrinetti P, Palenzona A, Putti M and Eibl O 2005 *Supercond. Sci. Technol.* **18** 572

[59] Yang H D, Liu H L, Lin J-Y, Kuo M X, Ho P L, Chen J M, Jung C U, Park M-S and Lee S-I 2003 X-ray absorption and optical spectroscopy studies of $(Mg_{1-x}Al_x)B_2$ *Phys. Rev.* B **68** 092505

[60] Zambano A J, Moodenbaugh A R and Cooley L D 2005 Effects of different reactions on composition homogeneity and superconducting properties of Al-doped MgB_2 *Supercond. Sci. Technol.* **18** 1411–20

[61] Karpinski J *et al* 2005 Al substitution in MgB_2 crystals: influence on superconducting and structural properties *Phys. Rev.* B **71** 174506

[62] Slusky J S *et al* 2001 Loss of superconductivity with the addition of Al to MgB_2 and a structural transition in $Mg_{1-x}Al_xB_2$ *Nature* **410** 343–5
[63] Zandbergen H W, Wu M Y, Jiang H, Hayward M A, Haas M K and Cava R J 2002 The complex superstructure in $Mg_{1-x}Al_xB_2$ at $x \approx 0.5$ *Physica* C **366** 221–8
[64] Agrestini S *et al* 2004 Substitution of Sc for Mg in MgB_2: effects on transition temperature and Kohn anomaly *Phys. Rev.* B **70** 134514
[65] Filippi M *et al* 2005 T_c as a function of electron doping in $Mg^{10}B_2$ using Sc for Mg substitution *J. Supercond.* **18** 667
[66] Filippi M, Agrestini S, Simonelli L, Saini N L, Bianconi A, De Negri S, Giovannini M and Saccone A 2007 XANES microscopy of phase separation in superconducting $Mg_{1-x}Sc_xB_2$ *Spectrochim. Acta* B **62** 717
[67] Stephens P W 1999 *J. Appl. Crystallogr.* **32** 281–9